# Chemistry with a sense of direction—the stereodynamics of bimolecular reactions

**Andrew J. Alexander, Mark Brouard, Konstantinos S. Kalogerakis and John P. Simons***

*The Physical and Theoretical Chemistry Laboratory, South Parks Road, The University of Oxford, Oxford, UK OX1 3QZ.*

**This review outlines some of the exciting new developments in the experimental study of the dynamics of elementary bimolecular reactions. Emphasis is placed on the 'new wave' of stereodynamical studies of photon initiated bimolecular reactions, using Doppler-resolved polarised laser pump and probe techniques. A few key studies, which are discussed in some detail, provide a taste of what has already been achieved, as well as a hint of the new experiments that can be anticipated in the near future.**

## 1 Introduction

The development of scientific innovation is often triggered by the advent of new experimental strategies which allow questions to be addressed by design rather than conjecture. At first, the new thinking is confined to a small group of laboratories but if the innovation is addressing important questions, the 'word soon gets around' and before too long, scientists in other laboratories or disciplines begin to get wind of the fact that something new and exciting is happening. This is the path that (may) lead one day, to Nobel prizes. When that day has come and gone, although a new sub-discipline has been created, the buzz may begin to subside and the new sub-discipline can become an esoteric speciality with its own high priests, language, priorities, biennial conferences—and even Review articles. A prime purpose of the present Review is to transmit some of the current buzz and passion which animates the (far from esoteric) world of molecular reaction dynamics; to show how some of the questions signalled by its Nobel Laureates can now be addressed using powerful new laser-based experimental strategies; and to report some of the extraordinarily detailed insights into the nature of chemically reactive collisions that are being revealed. The central challenge is easy to state, far less easy to achieve: it is to describe and understand the stereo-

*Dr Alexander gained his first degree, in Chemical Physics, from the University of Edinburgh in 1994 and his D.Phil. from the University of Oxford, working in Professor Simons' group, in 1997. He currently holds a post-doctoral research fellowship with Professor R. N. Zare in the Department of Chemistry, University of Stanford.*

*Dr Brouard obtained his D.Phil. from the University of Oxford in 1986, where he worked in the group of Professor M. J. Pilling in the field of gas phase reaction kinetics. He subsequently moved to Nottingham University, initially as a post-doctoral researcher in Professor Simons' group, and then, from 1989, as a University Lecturer. In 1993 he returned to the University of Oxford, where he is now a lecturer in the Department of Chemistry, and a Tutorial Fellow at Jesus College. His primary research interests in recent years have been in the fields of photodissociation and bimolecular reaction dynamics.*

*Dr Kalogerakis obtained his first degree in Chemistry from the University of Athens, Greece, in 1989, and his PhD from the University of Stanford, USA, working in Professor R. N. Zare's group, in 1995. He currently holds an EPSRC post-doctoral research fellowship with Professor Simons and Dr Brouard in the Department of Chemistry, University of Oxford, a College lectureship at Keble College, Oxford, and is a Junior Research Fellow at Worcester College, Oxford.*

*Professor Simons is the Dr Lee's Professor of Chemistry at the University of Oxford and a Professorial Fellow of Exeter College. He is a Fellow of the Royal Society, a past-President of the Faraday Division of the RSC, and a past-Chairman of the Molecular Beams and Dynamics and the Gas Kinetics Groups. He received the Tilden Lectureship in 1983, the Chemical Dynamics Award (sponsored by BP) in 1993, the Polanyi Medal and Lectureship in 1996 and presented the George C. Pimentel Memorial Lecture at Berkeley in 1998. He has been engaged in the study of molecular reaction dynamics and in particular, the stereodynamics of photon initiated reactions, for some thirty years.*

**Andrew J. Alexander**

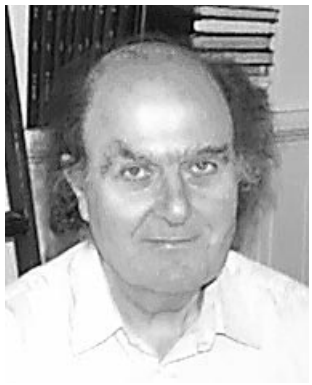

**John P. Simons**

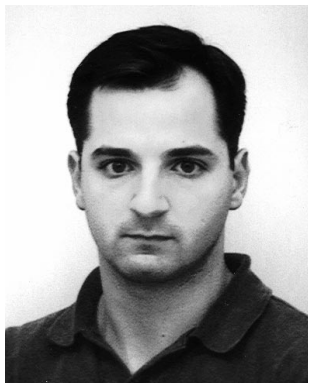

**Konstantinos S. Kalogerakis**

**Mark Brouard**

dynamics of a reactive molecular collision, to present a three-dimensional view of the passage through the transition state from reagents to products.

The most direct way of probing the stereodynamics of the collision is through monitoring the angular distribution, or better, the angle-resolved velocity distribution of the scattered products, best represented on a polar product scattering map. The most direct way of obtaining such a map is through monitoring the products scattered from two colliding reagent molecular beams using a (universal) mass spectrometer detector. Fig. 1 shows the scattering map for the abstraction reaction determined in this way by Y. T. Lee's group;[1] $|v', j'\rangle$ represent the vibrational and rotational levels of the nascent HF. It has become a famous picture, since almost uniquely, the kinematics of the reaction allow the angular distributions of each populated vibrational level, $v'$, in the scattered HF molecules to be separately resolved through their velocity spectrum. In the vast majority of cross-beam studies the angular distribution represents an average over *all* the populated product quantum states. For the F + $H_2$ reaction there is a switch from 'backward' to 'forward' scattering when the HF is excited into its highest, energetically accessible vibrational level, $v' = 3$. This subtle change, which would otherwise have been hidden, has taken a decade to understand and, in concert with *ab initio* theory and parallel studies of the photoelectron spectroscopy of the $FH_2^-$ anion, it has stimulated some of the most profound insights into the dynamics of a benchmark chemical reaction.[2]

$$F + H_2 \rightarrow HF|v', j'\rangle + H \qquad (1)$$

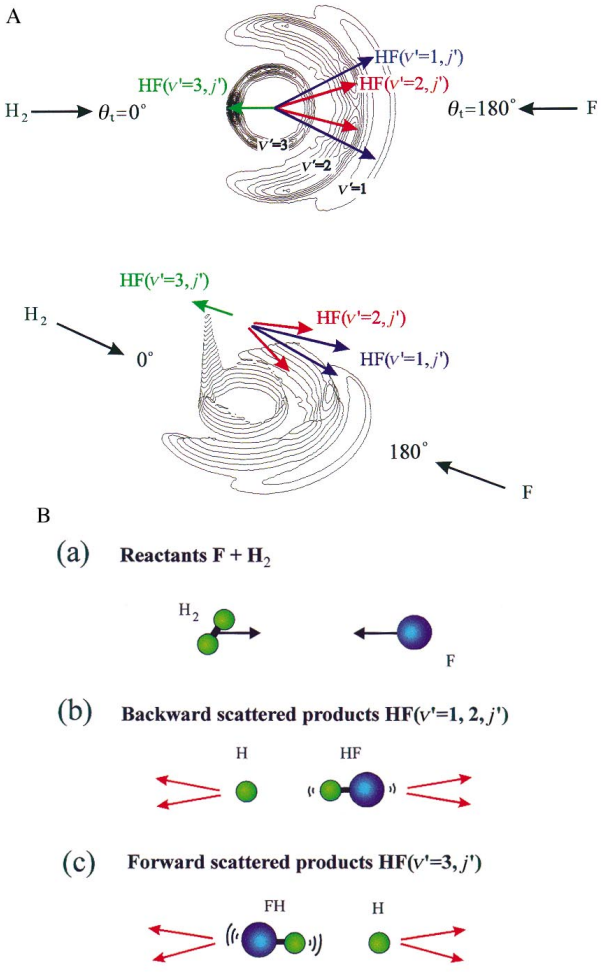


**Fig. 1** (A) A contour plot (upper panel) and a three-dimensional view (lower panel) of the scattering map for the F + $H_2 \rightarrow$ HF($v'$) + H reaction at a collision energy of 11.5 kJ $mol^{-1}$, adapted from reference.[1] The scattering into different product vibrational levels $v'$ is indicated. 0° corresponds to forward scattering with respect to the incoming F atom. (B) Schematic illustrations of the scattering behaviour shown quantitatively in part (A). Note, in particular, the contrasting scattering for HF molecules born in the $v' = 1,2$ and $v' = 3$ vibrational levels.

Optical detection provides an alternative to mass spectrometric detection; techniques such as tunable laser induced fluorescence (LIF) or resonantly enhanced multiphoton ionisation (REMPI) spectroscopy are both sensitive and, necessarily, product quantum state selective. If there is no population in the level being excited then of course, there is no signal! In principle, localised, angle- and time-resolved optical detection around the cross-beam scattering zone could provide a means of probing the distribution of the scattered products, but the dilution in their concentrations as they move away from the collision zone places severe demands on the detection sensitivity. Fortunately, there is an alternative approach which circumvents this difficulty—*Doppler-resolved* † optical detection of the scattered reaction products *at* the collision zone. Products moving towards or away from the detection laser experience a blue or red shift in their absorption spectra and their angle-resolved velocity distributions are 'encoded' in the Doppler contours of their spectral lines. This strategy, originally pioneered by Kinsey in the late 1970s,[3] provided the first, quantum state-resolved product angular distributions for a bimolecular reaction.

An elegant and visually appealing means to the same end couples selective laser ionisation at the scattering zone with angular imaging of the ionised product trajectories (which remain virtually undeflected by the loss of an electron), using a CCD camera. Transformation of the two-dimensional projections into three-dimensional angular distributions, generates a *family* of product-state resolved angular scattering maps.[4] These new experiments begin the process of resolving the swarm of successful (*i.e.* reactive) molecular collisions into their constituent sub-sets and exploring the dynamics of their individual classical trajectories; in quantum mechanical terms, the experiments begin the process of identifying individual elements in the reactive scattering matrix.

The process can be continued further by taking advantage of the *polarisation* of the probe laser beam to explore the spatial distribution of the *rotational* angular momentum, **j′**, of the scattered reaction products. In the classical limit of high $j'$, Q branch molecular transitions, with $\triangle j' = 0$, have their transition dipoles, $\boldsymbol{\mu}$, aligned parallel to **j′**; P or R branch features, with $\triangle j' = \pm 1$, have $\boldsymbol{\mu}$ directed perpendicular to **j′**.[5] In consequence the polarisation dependence of the Doppler-resolved laser induced excitation spectra reflects stereodynamic preferences in both the linear and the angular momentum spatial distributions, *e.g.* preferences for forward or backward scattering, or for 'cartwheel', 'discus' or 'propeller-like' rotational motion. The application of polarised, Doppler-resolved laser probe strategies has, more than any other, provided an especially high-powered lens through which the stereodynamics of individual molecular collisions may be viewed. . . . How was it created?

## 2 The vectorial approach

In a prescient paper[6] on the 'statistical theory of angular momentum polarisation in chemical reactions' published more than 20 years ago, Case and Herschbach wrote:

> 'directional or vector properties of chemical reaction dynamics contain much information not provided by energetic or scalar properties'

† We include under the heading of Doppler-resolved optical detection, REMPI techniques coupled with time-of-flight mass spectrometric detection. The important feature is that the optical technique must be sensitive to the (state-resolved) velocity distribution of the reaction product.

The paper was stimulated by a few pioneering experiments probing polarisation of rotational angular momentum from bimolecular scattering events. A few years later Case, McClelland and Herschbach noted[7]

> 'the wedding of lasers and molecular beams... now makes possible a wide variety of new experiments, particularly by means of laser induced fluorescence. . . . The method has great sensitivity and may allow the polarisation of individual vibration-rotation states to be measured as a function of the scattering angle'.

How right they were will become apparent as this review progresses, though it is only in the last year or so that the hope expressed in their second sentence has become an experimental reality.

A landmark conference, which was organised by Richard Bernstein, Dudley Herschbach and Raphael Levine in Jerusalem in 1986,[8] marked a turning point in the evolution of the study of reaction stereodynamics. One of its prime concerns was the measurement of the vector (spatial) correlations between **k**, **j**, **k′** and **j′**, the relative velocities and rotational angular momenta of the colliding or dissociating reagents and products and their analysis in terms of the stereodynamics they reflect. The power of polarised, Doppler-resolved probing in revealing the stereodynamics of molecular photodissociation[5] was already strongly apparent (following a key paper by Zare and Herschbach in 1963[5] and the subsequent development of the necessary analytical theory, during the 1980s, particularly by Greene and Zare[9] and Dixon[10]). Indeed, so successful had the strategy been that it distracted attention away from bimolecular reactions throughout most of the 1980s; it was not until the current decade that the balance was reversed, though the current 'new wave' of experiments leans heavily on the earlier studies of molecular photodissociation.

The most powerful strategy uses polarised photodissociation of an appropriate molecular precursor, to generate velocity aligned atomic or free radical reagent 'beams in a bulb'; the products scattered from their subsequent secondary collisions are probed by a second, tunable, polarised laser after a short delay (short enough to ensure 'single collision conditions' and the avoidance of subsequent collisional relaxation). The philosophy is best illustrated by one of the first pioneering experiments to be conducted in this way, in Richard Bersohn's laboratory at Columbia University.[11] They compared LIF Doppler-resolved profiles of (i), the H atoms generated by polarised photodissociation of the precursor molecule, $H_2S$ [reaction (2)], and (ii), the D atoms recoiling from their subsequent collision with the target molecule $SiD_4$ [reaction (3)].

$$H_2S + h\nu \xrightarrow{(193\ \text{nm})} H + HS \qquad (2)$$

$$H + SiD_4 \longrightarrow HSiD_3 + D \qquad (3)$$

The H atoms are generated with very high translational energy, in excess of 150 kJ mol$^{-1}$, and their velocity is aligned perpendicular to the polarisation vector **ε**, of the absorbed photons (since the electronic transition is polarised perpendicular to the molecular plane of the $H_2S$). H atoms recoiling perpendicular to **ε** present a double-peaked Doppler contour, reflecting their motion towards or away from the 'observer'; when the probe laser is directed parallel to **ε**, the Doppler profile narrows and only presents a single, central peak. Remarkably, the D atoms generated in the secondary reaction (3), present very similar behaviour—the D atoms tend to emerge with velocities directed parallel to those of the incident H atom, *i.e.* with **k** ∥ **k′**, but moving more slowly to conserve momentum. The results have been interpreted in terms of a displacement mechanism proceeding through transition state structures approximating a trigonal bipyramid, *i.e.* a 'collinear' inversion mechanism (reminiscent of an $S_N2$ reaction).[11]

This innovative experiment provided a flavour of the 'shape' of experiments to come but, despite its elegance, it was limited in its scope in two or three important respects. Since the centre-of-mass of the colliding reagents lies very close to the heavy target molecule the velocity of the centre-of-mass of the reaction system is very small. In consequence, the velocities (observed in the laboratory frame *via* the Doppler spectrum) of products scattered in the same direction as the reagent H atoms, *i.e.* forwards, are virtually the same as any that are scattered backwards. The interpretation in terms of forward scattering, although highly plausible, remains an interpretation. Secondly, the experiment was restricted to monitoring the atomic product, only.

The full flowering of the new strategy has not been slow, however, and in the last three years it has been applied at steadily evolving levels of refinement, to a wide range of bimolecular reactions. The measurement of both linear and angular momentum correlations in reactions involving both atomic and molecular reagents has provided a wealth of new dynamical information which either complements or supersedes that gained from crossed molecular beam studies. The developments foreseen by Case, McClelland and Herschbach over twenty years ago[7] are, at last, being realised; for illustrative examples, read the rest of this Review and, for alternative sources, see the excellent earlier reviews written by Orr-Ewing and Zare[12] and/or by (two of) the present authors[13] (the reader can judge as to the excellence of the latter).

## 3 The stereodynamics of photon initiated bimolecular reactions: concepts and machinery

### 3.1 The concept

Consider the idealised photon initiated reaction sequence[14,15] (4) and (5), in which monoenergetic, velocity aligned atomic

$$AD \xrightarrow{h\nu\ (\text{pol})} A_t + D \qquad (4)$$

$$A_t + BC|i\rangle \rightarrow AB|f\rangle + C \qquad (5)$$

reagents, $A_t$, generated in step (4), collide with a stationary target molecule, BC, in quantum state $|i\rangle$ to generate a product AB, in a quantum state $|f\rangle$, which is subsequently probed (state-selectively) *via* Doppler (or time-of-flight) resolved laser excitation. The Doppler broadened spectrum of the scattered products reflects their speed distribution in the reference frame of the observer, *i.e.* in the laboratory or LAB frame, but this speed distribution is determined by the dynamics of the collision in the molecular frame, referenced to the *relative* velocity of the reactants, **k**, with an origin at the centre-of-mass of the colliding reagents, *i.e.* the CM frame. If the reagent atom is moving much faster than the target molecule, the velocity of the centre-of-mass, $\mathbf{v}_{CM}$, will be given by eqn. (6).

$$\mathbf{v}_{CM} \simeq \left(\frac{m_A}{m_A + m_{BC}}\right)\mathbf{v}_A \qquad (6)$$

Fig. 2 presents simple velocity vector diagrams ('collapsed' Newton diagrams) for reactive collisions in which the molecular reagent velocity, $\mathbf{v}_{BC} \simeq 0$. The LAB frame velocities of products AB (or C) scattered at an angle $\theta_t$ and velocities $\mathbf{w}_{AB}$ (or $\mathbf{w}_c$) in the CM frame, will be given by eqn. (7). If the

$$\mathbf{v}_{AB} = \mathbf{v}_{CM} + \mathbf{w}_{AB} \text{ or } \mathbf{v}_C = \mathbf{v}_{CM} + \mathbf{w}_C \qquad (7)$$

products are scattered forwards, *i.e.* with $\theta_t \rightarrow 0°$, their LAB velocity will be enhanced by $\mathbf{v}_{CM}$; if they are scattered backwards their LAB velocity will be diminished by $\mathbf{v}_{CM}$ —the simple vector sum in eqn. (7) provides a means of establishing the full product angular distribution. The sensitivity is maximised when $v_{CM} = \omega_{AB}$ (or $\omega_C$). In the example of the H + $SiD_4$ reaction discussed above, reactive scattering of a light atom (H) by a heavy target molecule ($SiD_4$), $v_{CM} \ll \omega_C$, occurred, and it was not possible to distinguish between forward and backward scattering. Fortunately, however, this represents an extreme and rare situation.

The Law of Cosines is given in eqn. (8). If the kinetic energy

$$v_{AB}^2 = v_{CM}^2 + \omega_{AB}^2 + 2v_{CM}\omega_{AB}\cos\theta_t \quad (8)$$

of A, the internal energy of BC, and the exoergicity (*i.e.* the energy release) in the reactive collision (5) are known *a priori* (as they commonly are), and C carries no internal excitation, then selection of the product quantum state $|f\rangle$ will fix the kinetic energy of the scattered products and therefore the speed $\omega_{AB|f\rangle}$, through energy conservation. Under these conditions each laboratory speed, $v_{AB|f\rangle}$, maps uniquely onto a centre-of-mass scattering angle $\theta_t$ (see Fig. 2), and the LAB speed distribution determined from the Doppler spectrum provides the state-selected product scattering angular distribution in the CM frame, $P(\theta_t)$, proportional to the state resolved differential cross-section. In a less than ideal world, of course, the method is not quite that simple but the central concept is sustained.

### 3.2 The unobserved products

In the vast majority of reactions, the constraint limiting the (usually) *un*observed product C of the bimolecular reaction (5) to a structureless atom will not operate. Even when C is monatomic, it is likely to be an open shell atom, the energy of which may well be split through spin-orbit interaction, *e.g.* $I(^2P_{3/2})$ and $I(^2P_{1/2})$. If the unobserved product is molecular, as, for example, in a reaction of type (9), it will be generated in a

$$A_t + BCD \rightarrow AB|f\rangle + CD|f'\rangle \quad (9)$$

range of ro-vibrational states, and the monitored products AB $|f\rangle$, will be scattered with a corresponding spread of kinetic energies/velocities, $\omega_{AB|f\rangle}$. Under these, more general circumstances, the AB product speed distribution in the LAB frame will reflect both the CM angular distribution (the AB$|f\rangle$ state-resolved differential cross-section) *and* the kinetic energy distribution (reflecting the internal energy distribution in the *correlated* partner). Were this the end of the story, there would be less to relate, but fortunately, the increased complexity also offers increased opportunity since there are ways of extracting both the angular distributions and the correlated kinetic energy distributions from the Doppler-resolved spectra.[16–18] The key lies in taking advantage of measurements using alternative detection geometries, *e.g.* with the photolysis and detection beams aligned either parallel or perpendicular to each other and with the further option of a parallel or perpendicular alignment of their polariisation vectors. The alternative geometries allow the scattered products to be 'viewed' from different perspectives in the LAB frame.

An example set of results derived in the above fashion is shown in Fig. 3. The data are for the OH products of the H + $CO_2$ reaction,[17] and are plotted as a scattering map, representing the joint distribution of the CM speed ($\omega_{AB|f\rangle}$) and scattering angle (cos $\theta_t$) of the OH. Although the scattering map is reminiscent of that shown for F + $H_2$ in Fig. 1, the new map shown in Fig. 3 corresponds to the scattering of a *specific* product OH quantum state ($v' = 0$, $N = 5$). Furthermore, measurement of the product speed distribution, together with the constraint of energy conservation, allows the correlated kinetic energy (or product speed) distribution to be converted into the correlated *internal* energy distribution $P(E_{f'})$, in the *un*observed products which accompany AB$|f\rangle$.

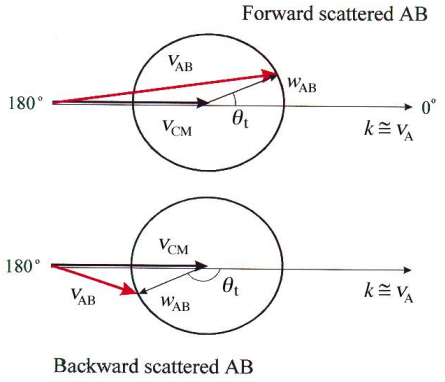


**Fig. 2** 'Collapsed' Newton diagrams for the situation in which the velocity of the target molecule can be neglected, *i.e.* $v_{BC} \simeq 0$. CM scattering into the forward (upper figure) and backward hemispheres (lower figure) leads to different product speeds, $v_{AB}$, in the laboratory frame. $v_{CM}$ is the velocity of the centre-of-mass, and $w_{AB}$ is the AB product velocity in the CM frame.

### 3.3 Rotational polarisation: product angular momentum distributions

As well as reflecting the (vectorial) angle-resolved velocity distributions of the scattered reaction products, and the (scalar) product internal quantum state distributions, the Doppler (or REMPI time-of-flight) contours also reflect a third dynamical factor—the state-resolved product angular momentum distributions.[6,7,12–14,19–21] Their influence is imaged, in the LAB frame, by the dependence of the Doppler broadened spectrum on the rotational polarisation of the scattered products. If the state-resolved product angular momentum distributtion is anisotropic (*i.e.* polarised) in the LAB frame, both the intensity and the shape of the Doppler spectrum will vary with the experimental configuration and the type of rotational transition selected by tuning the probe laser, *e.g.*, Q ↑ or P, R ↑ .

To appreciate the dynamics properly, however, they need to be viewed through the 'molecule's eye', *i.e.*, in the molecular or CM frame, which has its *z*-axis parallel to the relative velocity of the reactants; in this frame the laboratory velocities are replaced by the relative velocities **k** and **k′**, and the **k**, **k′**, **j′** distribution can be defined in terms of the angles shown in Fig. 4. $\theta_t$ represents the scattering angle between the reagent and product velocity vectors, **k** and **k′**. A preference for $\theta_t \rightarrow 0°$, for example, would indicate forward scattering in the CM frame; a preference for $\theta_t \rightarrow 180°$ would indicate backward, or 'rebound' dynamics. The angles $\theta_j$ and $\phi_j$ are the polar and azimuthal angles of the rotational angular momentum **j′**, referenced to the reagents velocity **k** and the scattering plane (**k**, **k′**). A distribution peaking at ($\theta_j$, $\phi_j$) = (90°, 90°) or (90°, 270°) for example, would reflect a preference for the products to spin away from the reactive collision like a frisbee or discus; a distribution peaking at ($\theta_j$, $\phi_j$) = (90°, 0°) could indicate either

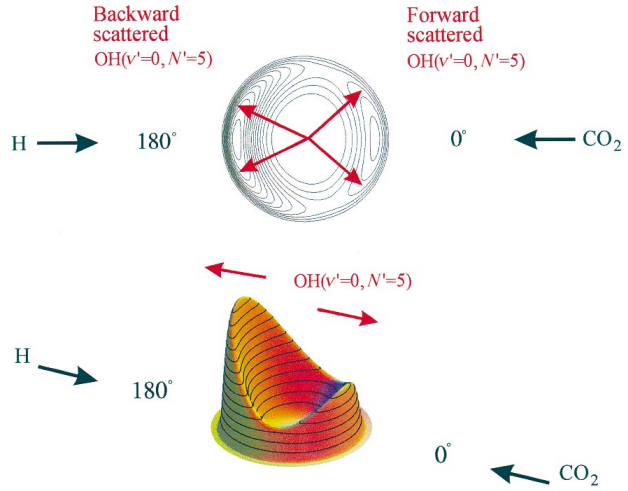


**Fig. 3** A contour plot (upper figure) and three-dimensional view (lower figure) of the product scattering map for the reaction H + $CO_2 \rightarrow$ OH($v' = 0$, $N' = 5$, $A'$) + CO at a mean collision energy of 240 kJ mol$^{-1}$, adapted from reference.[17] The data reveal a forward-backward peaking product angular distribution, with a bias in the backward direction, and a broad OH($v' = 0$, $N' = 5$, $A'$) CM speed distribution, which peaks at high OH speeds. This speed distribution reflects the internal energy distribution in the CO co-products to OH($v' = 0$, $N' = 5$, $A'$), which, from energy conservation, must be born internally cold.

a preference for cartwheel motion or propeller-like motion, depending on the preferred scattering angle $\theta_t$.

The full CM angular distribution of **k**, **k′** and **j′** is expressed in terms of three angles, *i.e.* $P(\theta_t, \theta_j, \phi_j)$; it describes the dependence of the angular momentum polarisation on the CM scattering angle.[6,7] When integrated over scattering angle, the resulting (scattering angle averaged) rotational angular momentum distribution, $P(\theta_j, \phi_j)$, can be displayed in the form of a polar map—a typical example, taken from classical trajectory data for the F + $H_2$ reaction,[22] is shown in Fig. 5.

The full CM angular distribution may be written (semi-classically‡) in terms of expansions either in bipolar or spherical harmonics.[12,19,20] The 'moments' or coefficients defining these expansions are known either as the *polarisation dependent differential cross-sections*[19] (PDDCS's) or the related *bipolar moments*.[20] Only the low order moments of the angular momentum polarisation distribution can be extracted from the dependence of the Doppler contours on pump-probe geometry and rotational transition.[20,21] Low order even *alignment* moments are obtained using linearly polarised probe laser radiation, whilst low order odd *orientation* moments may, in principle, be determined using circularly polarised light.

### 3.4 Transformation from the LAB frame to the CM frame

Transformation of data obtained in the experimental laboratory frame to the molecular, centre-of-mass frame can be effected through a least squares fitting procedure, based upon a set of basis functions,[24] which depend parametrically, on the angles of interest. The simplest example reflects the correlation between **k** and **k′**, *i.e.* the conventional differential cross-section determined by the angular distribution in $\theta_t$. An example basis set which was used to analyse the dynamics of reaction (10) is

$$H + CO_2 \rightarrow OH + CO \qquad (10)$$

shown in Fig. 6; the basis functions depend parametrically on $\theta_t$ and the energy $E'_t$, released into translation in the scattered

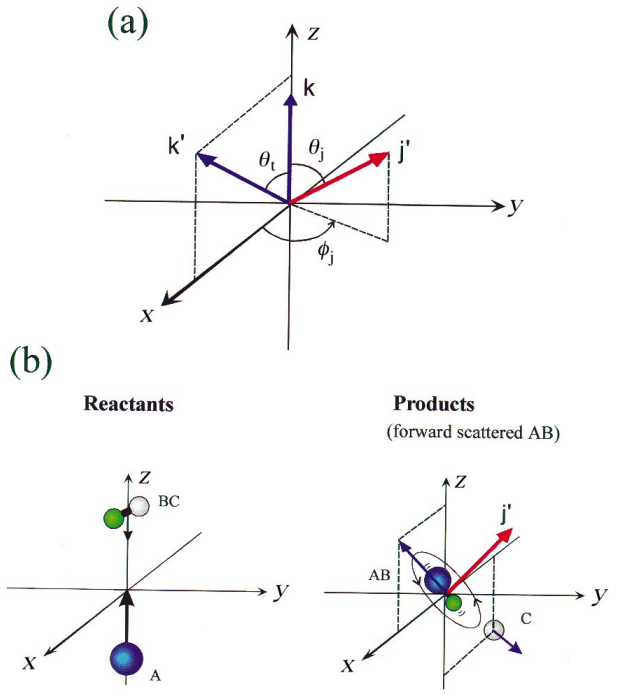


**Fig. 4** (a) The definition of the scattering angle $\theta_t$, and the polar angles $\theta_j$, $\phi_j$, which define the direction of **j′** with respect to the **k**–**k′** scattering plane. In part (b), these definitions are illustrated for AB products rotating and scattering in the particular directions shown. The reactant relative motion defines the CM *z*-axis (see the left figure), and the *xz* plane is defined by the relative motion of the product molecules (right figure).

‡ A comprehensive quantum mechanical treatment of angular momentum polarisation in elementary bimolecular reactions has recently been given by Miranda and Clary.[23] This paper also contains an excellent review of angular momentum polarisation in elementary chemical reactions.

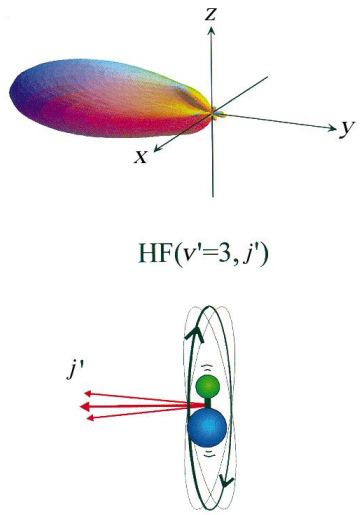


**Fig. 5** An example of a polar plot of the angular momentum polarisation for the F +$H_2$($v$ = 0, $j$ = 0) → HF($v'$ = 3) + H based on the classical trajectory calculations presented in reference 22. The upper figure shows the full distribution, employing an expansion in seven moments. The lower figure illustrates the *oriented* rotational motion of the vibrationally excited HF products. As shown in Fig. 4, the centre-of-mass frame *xz* plane corresponds to the scattering plane, and thus contains the HF product relative velocity vector. Recall that the particular HF($v'$ = 3) products in question are scattered in the forward direction (see Fig. 1), *i.e.* with velocity vectors lying nearly parallel to the *z* axis.

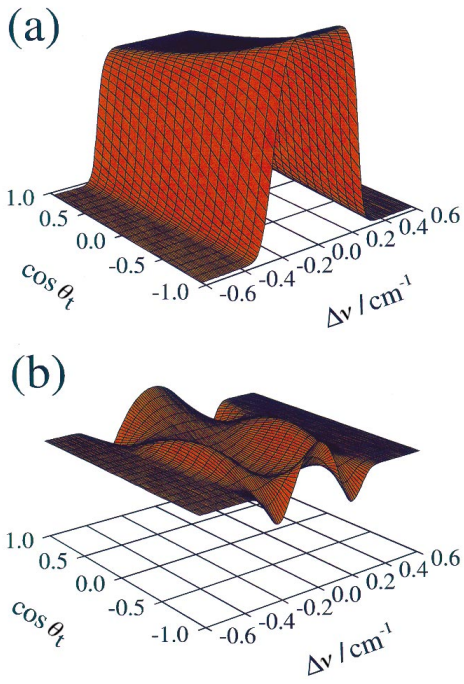


**Fig 6** Example basis functions for the H + $CO_2$ reaction at a mean collision energy of 240 kJ mol$^{-1}$. Only the dependence on CM scattering angle, $\theta_t$, is shown, for a fixed value of the fractional kinetic energy release, $f_t$ = 0.725. The basis functions were employed to fit the sum (a) and difference (b) of experimental Doppler profiles obtained in parallel and perpendicular pump-probe geometries. Those shown in (a) depend only on the OH speed distribution in the LAB frame, whilst those in (b) depend on the OH LAB frame translational anisotropy. The derived CM polar scattering map has already been shown in Fig. 3.

products (expressed as the fraction $f_t \equiv E'_t/E_{total}$), which itself is determined by the internal energy distribution in the unobserved CO fragment. The corresponding polar scattering map derived from fits to experimental data has already been shown in Fig. 3. The state-resolved differential cross-sections may, and generally do, depend on the selected product channel, and thereby reflect the detailed anatomy of the reactive collisions. Cross-beam scattering experiments, which employ conventional time-of-flight mass spectrometry rather than optical spectroscopy, are generally far more limited in their scope.

It is possible to extend the basis function strategy to determine additional parameters, for example, the collision energy dependence of the reaction probability, measured by the reaction cross-section $\sigma_R(E_t)$,[25] or the rotational polarisation of the scattered products, reflected in the sensitivity to the choice of detection *via* $Q\uparrow$ or P, $R\uparrow$ probe transitions.[17] The most powerful formulations enable a set of polarisation dependent differential cross-sections to be determined from which the low order moments of the full spatial distribution of the products linear and angular momenta, $P(\theta_t, \theta_j, \phi_j)$, can be determined[17,21,26,27]—realising the dream expressed by Case, McClelland and Herschbach more than 20 years ago[8]

### 3.5 A few caveats

In general, the contours of the Doppler broadened product spectra can be influenced by a range of factors, some of which can be controlled by the experimenter and some of which reflect the dynamical behaviour of the reactive collisions, *i.e.* what is actually sought. The former (may) include:

i The thermal spread of velocities in the reagent source and the molecular target;[14,28] these can be accommodated by appropriate averaging or virtually eliminated, by co-expanding the source and target molecular reagents in a supersonic nozzle expansion.

ii The spread in the internal quantum states of the molecular reagent; these too, can be constrained by nozzle beam expansion or (so far, rarely) the reagent may be state selected through prior optical excitation.

iii A spread in the collision energies, associated with the dynamics of the photon initiation step, *e.g.* when the source is a polyatomic molecule. This can be accommodated either by assuming the dynamics/cross-section of the subsequent bimolecular reaction to be insensitive to the spread of collision energies or better, by making a virtue of necessity and using the (known) spread to explore the energy dependence[25] or better still, by choosing (if possible) an alternative mono-energetic but 'tunable' photolytic source.

## 4 Case histories

### 4.1 Overview

The ability to determine the distributions of linear and rotational angular momenta among the quantum state-resolved products of reactive molecular collisions represents, literally, a quantum-jump in our ability to penetrate the microscopic world of chemical reaction dynamics. Their interpretation in the light of accurate quantum scattering and/or quasi-classical trajectory (QCT) calculations on reliable, *ab initio* potential energy surfaces, provides a profoundly detailed view of the dynamics of reactive molecular collisions; witness the recent triumphs in understanding the dynamics of the reactions of H(D) and F with $H_2$ and its isotopes.[2] The development of polarised, Doppler-resolved, optical detection methods has provided a new and extremely powerful general strategy towards the dynamicists' ultimate objective—a full three-dimensional perspective of the stereodynamics of individual reactive collisions. The remainder of this Review provides a flavour of some of the prizes that have already been won (hard-won) through their application.

Early intimations of what was to come arrived at the start of the decade, with the studies of Bersohn and his co-workers[11]—the first to exploit the anisotropy of molecular photodissociation to probe the dynamics of a subsequent secondary reaction, *e.g.* the displacement reaction (11), see Section 2. These studies

$$H + CD_4(SiD_4) \rightarrow CD_3H(SiD_3H) + D, \quad (11)$$

were followed rapidly by new experiments which utilised Doppler resolved, polarised laser detection to probe the full range of state-resolved (**k**, **k′**, **j′**) correlations among the scattered molecular products of reactive collisions. Examples include reactions (12)–(21), many of which have either been mentioned already or were discussed in earlier reviews, where further leading references can be found.[12,13] Reaction (21), the first to employ both product and reagent state selection, will be discussed in more detail in Section 4.2.

$$O(^1D) + N_2O \rightarrow NO|f\rangle + NO|f'\rangle \text{ (ref. 13)} \quad (12)$$

$$O(^1D) + H_2{}^{18}O \rightarrow OH|f\rangle + {}^{18}OH|f'\rangle \text{ (ref. 13)} \quad (13)$$

$$H + O_2 \rightarrow OH|f\rangle + O \text{ (ref. 24)} \quad (14)$$

$$O(^1D) + HCl \rightarrow OH|f\rangle + Cl \text{ (ref. 25)} \quad (15)$$

$$O(^3P) + CS \rightarrow CO|f\rangle + S \text{ (ref. 29)} \quad (16)$$

$$O(^3P) + H_2S \rightarrow OH|f\rangle + HS \text{ (ref. 29)} \quad (17)$$

$$H + CO_2 \rightarrow OH|f\rangle + CO \text{ (ref. 17)} \quad (18)$$

$$H + H_2O \rightarrow OH|f\rangle + H_2 \text{ (ref. 18)} \quad (19)$$

$$O(^1D) + CH_4 \rightarrow OH|f\rangle + CH_3 \text{ (ref. 16)} \quad (20)$$

$$Cl + CH_4|i\rangle \rightarrow HCl|f\rangle + CH_3 \text{ (ref. 15)} \quad (21)$$

The pioneering studies of reactions (14)[24] and (20)[16] provided the first examples of reactive collisions proceeding through (potentially) bound intermediates, respectively $HO_2$ and $CH_3OH$ formed through addition or insertion. In each case, a detailed analysis of the polarisation-dependent, Doppler-resolved laser induced fluorescence of the scattered OH products, provided a rich foretaste of the delights to come. The OH radical (like NO) is wonderfully equipped to act as an eloquent reporter of the stereodynamics involved in its formation. Its ground electronic state carries both spin and electronic orbital angular momentum and its fluorescent electronic transition, $A^2\Sigma \leftarrow X^2\Pi$, presents both Q and P,R branches to allow a full determination of the vectorial distribution of **k**, **k′**, **j′**. Furthermore, the coupling of its molecular rotation, *j′*, with its electronic orbital angular momentum, $\Lambda$, splits each rotational level into two components, known as 'lambda doublets'. They can be identified with radicals in which the odd electron occupies either the $\pi$-orbital lobe directed perpendicular to the rotation plane, $\pi(A'')$, or the lobe lying in the rotation plane, $\pi(A')$, see Fig. 7. Their unequal population would reflect a propensity for *electronic orbital alignment* and perhaps, an insight into the electronic motion within the collision complex.

Initially, it was thought that the vector correlations associated with the nuclear motions, *i.e.* those involving **k**, **k′** and **j′**, would be independent of those involving the electronic motions, but it was not to be. The first clue came in analysing the Doppler contours of OH scattered from the reaction of H with $O_2$ [reaction (14)]. It simply was not possible to obtain consistent results unless the OH products scattered into the two alternative lambda-doublet states were endowed with different rotational polarisations: 'frisbee-like' for the $\pi(A')$ states but isotropic for the $\pi(A'')$ partners.[24]

### 4.2 Some case studies: the state-of-the-art

Some of the most recent optical studies of the stereodynamics of bimolecular reactions have been conducted in Oxford, and in

Stanford by Richard Zare's group; they provide excellent illustrations of the present state-of-the-art. Key studies include the reaction of atomic chlorine with methane and ethane and some of their deuterated isotopomers,[21,27,30] and of electronically excited oxygen atoms $O(^1D_2)$ with hydrogen and methane.[16,26,31]There are fundamental differences in the way the two reagents interact in reactions (22) and (23), which are associated with the differing topography of the potential energy surfaces that the two attacking atoms encounter when they approach the C–H (or H–H) bond. In reaction (22) the chlorine atoms prefer to attack at the H atom end of the bond and need to surmount an energy barrier for the reaction to proceed; the net process is an endothermic, 'abstraction' reaction. In contrast, singlet oxygen atoms prefer to attack the H–H or C–H bond 'side-on' and 'insert'; reactions (23) and (24) are strongly exothermic and proceed over a deeply attractive potential energy surface (correlating with $H_2O$ or $CH_3OH$) which presents little or no barrier to the approach of the oxygen atom (see Fig. 8). The strikingly different mechanisms for the Cl and $O(^1D_2)$ atom reactions are reflected in their own characteristic stereodynamics.

$$Cl(^2P_{3/2}) + CH_4 \rightarrow HCl|v' = 0, 1, j'\rangle + CH_3 \qquad (22)$$

$$O(^1D_2) + CH_4 \rightarrow OH|v' \leqslant 4, j'\rangle + CH_3 \qquad (23)$$

$$O(^1D_2) + H_2 \rightarrow OH|v' \leqslant 4, j'\rangle + H \qquad (24)$$

That is not the whole story, however, since the $O(^1D_2)$ atom may also have an opportunity to interact with the target molecule over one (or more) *electronically excited* potential energy surface(s), correlating with dissociative, electronically excited states of $H_2O$ or $CH_3OH$.[31–33] On its own, the $O(^1D_2)$ atom is five-fold degenerate but, under the lowered symmetry of the collision, this degeneracy is lifted. For $O(^1D) + H_2$, the lowest of these in a linear configuration, designated $^1\Sigma$, would correlate with the ground state of water, but the next two, $^1\Pi$ and $^1\Delta$, correspond to electronically excited states. *Ab initio* computations of the $^1\Pi$ surface (which splits into $^1A'$ and $^1A''$ surfaces in a bent collision complex), indicate a small energy barrier for near collinear configurations and a surface topography closely resembling that for the interaction of $H_2$ with the halogen atoms, F or Cl (one up from O in the Periodic Table), see Fig. 9. If the collision energy is high enough to surmount the low entrance barrier, abstraction could begin to compete with insertion. But that may not be the whole story either. . . ! There is a possibility that collisions initially governed by one potential energy surface may switch 'their allegiance' to another at shorter range. The surfaces may intersect, allowing reactive collision trajectories to 'hop' from one surface to another: if this occurs, some collisions which started out on an 'abstractive' pathway over an excited energy surface might still end up on an 'insertion' pathway proceeding over the ground state surface. Molecular reaction dynamics can be a subtle business.

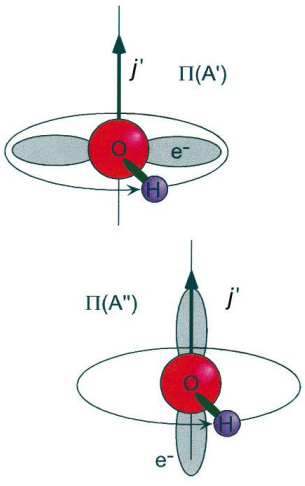


**Fig. 7** The limiting high $j'$ unpaired electron density in the A′ and A″ lambda-doublets in the ground $^2\Pi$ state of OH. Q ↑ transitions probe the A″ level, while P/R ↑ transitions probe the A′ lambda-doublet level.

### *4.2.1 The reaction of Cl with $CH_4$*

The reaction of $Cl(^2P_{3/2})$ atoms with $CH_4$ (in its vibrational ground state), reaction (22), is endothermic ($\Delta H^{\ominus}(0\ K) = +7.9$

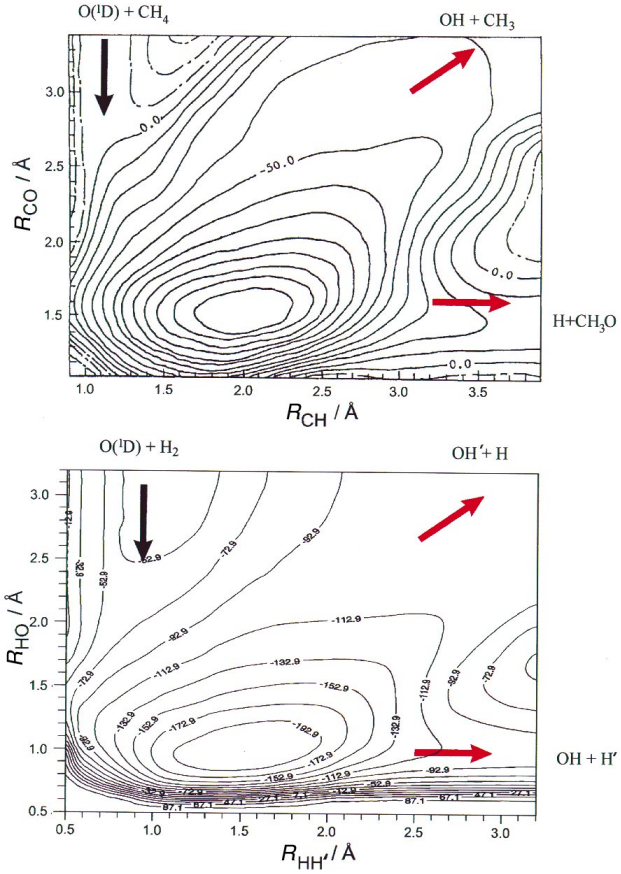


**Fig. 8** Sections through the potential energy surfaces for the reactions of $O(^1D)$ with $CH_4$[33] (upper panel) and with $H_2$ (lower panel).[32] The reactant valley in both figures is on the upper left and is shown by the black arrow. Two alternative product channels are shown as red arrows.

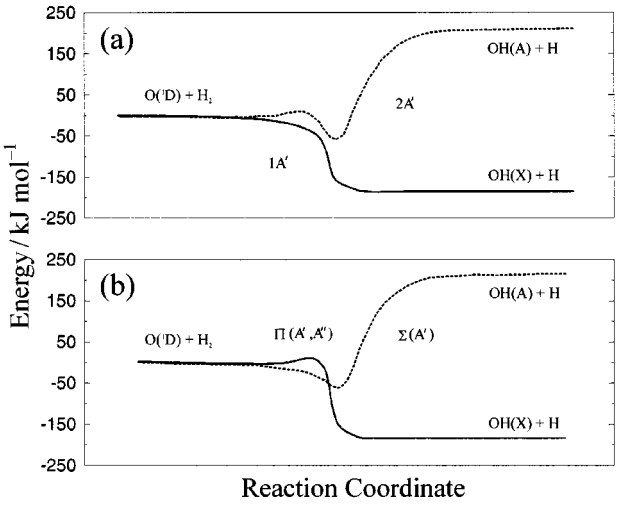


**Fig. 9** The variation of the potential energy along the reaction coordinate for the 1A′, 2A′ and A″ electronic states of the $O(^1D_2) + H_2$ reaction, adapted from Fig. 1 of Schatz *et al.*, *Faraday Discuss. Chem. Soc.*, **108**, reference 32. The curves shown in (b) are for collinear O–H–H configurations, while those in (a) are for bent O–H–H.

kJ mol$^{-1}$); in addition, there is also a considerable energetic barrier to reaction (*ca.* 15 kJ mol$^{-1}$) which limits the reaction probability, measured by its reactive cross-section, $\sigma_R$. The cross-section can be enhanced by increasing the collision energy or, much more effectively, through vibrational excitation of the $CH_4$; the effect of reagent vibrational excitation on the reaction stereodynamics has been investigated by Zare and co-workers,[15,30] using infra-red (IR) laser radiation to excite one quantum of the asymmetric stretching mode ($v_3 = 1$). The two reagents, $Cl_2$ and $CH_4$, were co-expanded as a 'mixed' molecular beam in helium (to minimise the effects of thermal motion on the spread of reagent velocities) and crossed with an IR laser beam, tuned to excite the transition, $v_3 = 0 \rightarrow 1$ in the $CH_4$. The abstraction reaction (22) was initiated by photolysis of the $Cl_2$, using a second, linearly polarised UV laser operating at 355 nm, which produces a velocity-aligned pulse of $Cl(^2P_{3/2})$ reagent atoms. After a delay of a few tens of nanoseconds the $HCl|v', j'\rangle$ products were interrogated by a third tunable (REMPI) laser pulse, which selectively ionised the products from the specifically populated rovibrational states, $|v', j'\rangle$. Their velocity distribution was measured by recording the time-of-flight of the $HCl^+$ ions to a remote detector employing a strategy known as 'core extraction',[15] which differs a little from the Doppler technique described earlier. However, using analogous procedures to those outlined in Section 3, the LAB frame velocity distribution of the state-selected reaction products could be converted into a family of (state-resolved) angular distributions, see Fig. 10, referenced to the relative velocity of the reagents—the key step which provides the first direct insight into the dynamics of the reactive collisions and of the molecular interactions which govern them.

The experimental results were intriguing: HCl products generated in $|v' = 0$, high $j'\rangle$ were scattered backwards and sideways with respect to the velocity of the incoming Cl atom. In contrast, the HCl molecules generated in $|v' = 1, j'\rangle$, were scattered predominantly forward, for products with low rotation, but shifted towards the backward hemisphere as the product rotation increased. Very similar results were obtained when $CD_3H$ was substituted for $CH_4$, suggesting a 'spectator' role for the unobserved partner fragments, $CH_3$ or $CD_3$. The results could be understood if HCl $|v' = 1$, high $j'\rangle$ products were generated by near head-on, 'hard-sphere' collisions of Cl with the H–C bond, leading to backward or 'rebound' scattering, while the HCl $|v' = 0$, high $j'\rangle$ was associated with more 'glancing' trajectories (see Fig. 11). Forward scattered products, $HCl|v' = 1$, low $j'\rangle$, were generated through peripheral, or tangential collisions in which the C–H bond was oriented perpendicular to the velocity of the incoming Cl atom. A similar dynamical mechanism, described as 'peripheral abstraction', had been encountered earlier in a study of the $O(^1D_2) + N_2O$ reaction.[13] This interpretation was confirmed by using a polarised IR laser to pre-orient the C–H bond axis through excitation of the symmetric C–H stretch mode, $v_1$, in the 'designer' target molecule $CD_3H$.[30] The photolysis laser polarisation could also be used to control the direction of the (velocity-aligned) Cl atoms and it was possible, therefore, to align the vibrating C–H bond either parallel or perpendicular to the reagent Cl atom velocity. As expected, the switch from an 'end-on' to a 'side-on' collision geometry enhanced the level of forward scattering from $CD_3H(v_1)$, in agreement with the mechanism proposed.

These quantum state-dependent, scattering angular distributions provide a uniquely resolved dynamical picture of the full ensemble of reactive molecular collisions, detail that would have been washed out if the HCl products had been detected without distinguishing the individual rovibrational states, *c.f.* a conventional crossed molecular beam experiment. In effect, the spread of product state-resolved angular distributions reflects the range of initial collision conditions, and the 'accuracy' of the initial collision trajectories, *i.e.* how closely they approach the target molecular 'bull's eye', measured by the *impact parameter*, *b*, and its direction or angular orientation. The HCl generated through reaction with vibrationally *un*excited $CH_4$ was generated exclusively in $|v' = 0\rangle$ with low rotational excitation and predominantly backward scattered. This was attributed to a 'tightening' of the conditions for reactivity to collision trajectories oriented along the H–$CH_3$ axis with low impact parameters (*i.e.* near direct hits). The angular spread of successful collision trajectories, *i.e.* the target molecule's 'cone-of-acceptance', widens when the molecule is vibrationally activated.

### *4.2.2 The reaction of $O(^1D_2)$ with $H_2$ and $CH_4$*

The reaction of electronically excited singlet oxygen atoms with $H_2$) reaction (24), is strongly exothermic [$\Delta H^{\ominus}$ (0 K) = −182 kJ mol$^{-1}$] and at room temperature, where the mean collision energies are low (*ca.* 3.6 kJ mol$^{-1}$), reaction over the ground state potential energy surface will be dominant since the surface presents no barrier. Not surprisingly, the reaction has a very

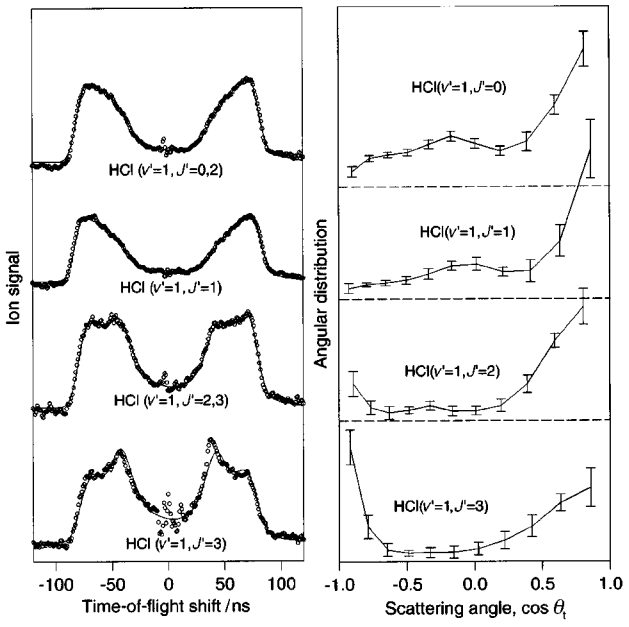


**Fig. 10** Experimental HCl($v' = 1, j' = 0$–3) product state-specific time-of-flight spectra (left panel), together with the fits to the data (solid lines) and the derived CM angular distributions (right panel) for the reaction Cl + $CH_4(v'_3 = 1) \rightarrow HCl(v'_3 = 1, j' = 0$–3) + $CH_3$. The figure is adapted from reference 30.

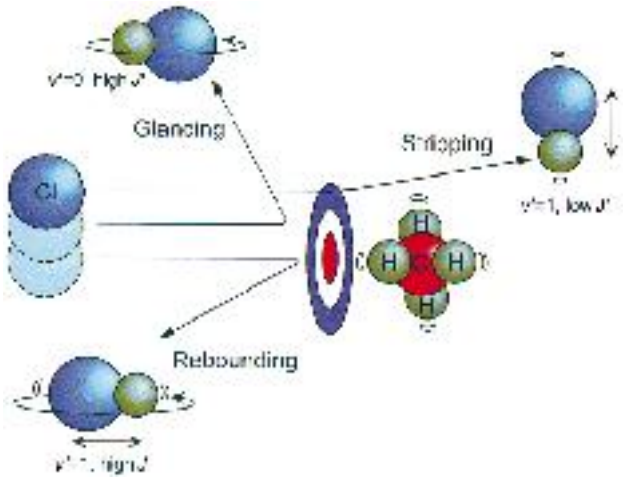


**Fig. 11** Schematic illustration of the contrasting reaction dynamics leading to HCl products in $v' = 0$ and $v' = 1$ in low and high $j'$ levels, for the Cl + $CH_4(v_3 = 1)$ reaction. The figure is adapted from reference 30. Some of the experimental data on which the figure is based is shown in Fig. 10.

high rate constant at room temperature. The OH fragments tend to spin away from the collision with high rotational angular momentum, $j'$, and all the energetically accessible vibrational levels, OH($v' = 0 \rightarrow 4$) are populated.

The angular distribution of the scattered products was first measured at Berkeley, by Yuan Lee and his co-workers[34] using the method of crossed molecular beams, coupled with mass spectrometric detection. The distribution, necessarily averaged over all product quantum states, was nearly symmetric, with peaks in both the forward and backward hemispheres—referenced to the incoming reagent oxygen atom. Among other possibilities, this could be interpreted to indicate the existence of a transiently bound rotating, ($H_2O$) collision 'complex', with a sufficiently long average lifetime, $\langle\tau_d\rangle$, with respect to its rotational period, $\langle\tau_r\rangle$, to result in a scrambling of the angular distribution, *i.e.* with no preference for either of the forward or backward directions (symmetric about $\theta_t = 90°$). The rotation, derived from the orbital angular momentum of the collision partners, would be expected to be fast, with a period in the femtosecond regime, in view of the low moment of inertia of the ($H_2O$) complex. Subsequent calculations using classical mechanics to simulate the ensemble of reactive collision trajectories on a computed *ab initio* potential energy surface, confirmed this time-scale, but also indicated a somewhat more complicated story.[13,31] Fig. 12 shows the predicted, *state-resolved* angular distributions of the products OH $|v', j'\rangle$ for two different vibrational quantum states, $|v'\rangle$. Products generated in $|v' = 4\rangle$ are predicted to be symmetrically distributed but those formed in $|v' = 0\rangle$ are mainly *backward* scattered.

Shortly after these calculations were published, the first state-resolved experimental study of the reaction was reported, using the newly-developed strategy of photon initiated reaction, using $N_2O$ as the photolytic source of O($^1$D), and optical state-resolved detection of the OH$|v', j'\rangle$ products.[31] Since the scattered reaction products are probed using *polarised* laser radiation, and the measurements are Doppler selective, they are sensitive both to the velocity *and* the rotational polarisation of the individually state-selected products, allowing the construction of a unique map of the correlated vectorial distribution between the reagent velocity, **k**, and the products' velocity and rotational angular momentum, **k′** and **j′**, in the aftermath of the reaction. Fig. 13 shows the results for **k**, **k′**: the angular distributions for the OH products formed in $|v' = 0, j' = 5$ or $14\rangle$ show a preference for backward scattering, in good agreement with the predictions of classical trajectory simulation.[26,31]

Similar experiments have also been conducted for the analogous reaction of O($^1$D) atoms with $CH_4$, reaction (23).[16] This system is more 'user-friendly' since the scattered products, OH and $CH_3$, with almost the same relative molecular mass, separate with equally fast velocities, in marked contrast to the product pair OH and H, where momentum conservation greatly constrains the velocity of the OH. The experimental scattering maps for OH$|v' = 0, j' = 5\rangle$ and OH$|v' = 4, j' = 8\rangle$, shown in Fig. 14, can be compared with the corresponding maps for the reaction of O($^1$D$_2$) with $H_2$ presented in Fig. 12. The similarities are striking. The scattering maps for OH$|v' = 0\rangle$ both display a strong backward peak and a weak forward peak while those for OH$|v' = 4\rangle$ both approach forward-backward symmetry. The correlations between the incoming and outgoing relative velocity vectors, **k**, **k′**, *i.e.* the scattering distributions, are remarkably similar for the two reactions, not surprisingly perhaps, in view of the similarity of their potential energy surfaces, shown in Fig. 8. The *scalar* energy correlations for the channels producing OH$|v' = 0\rangle$ are very different for the two reactions, however, since the kinetic energy released to the OH$|v' = 0\rangle$ from the reaction of O($^1$D$_2$) with $CH_4$ is remarkably low: most of the exoergicity appears as *internal* excitation of the (unobserved) polyatomic $CH_3$ fragment, implying that a considerable redistribution of vibrational energy takes place during the lifetime of the transient ($CH_3OH$) complex, $\langle\tau_d\rangle$, a lifetime that is shorter than its mean rotation period, $\langle\tau_r\rangle$. The

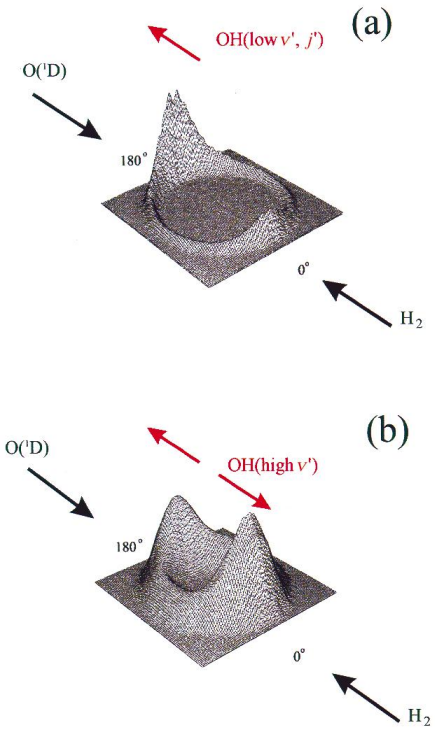


**Fig. 12** The QCT derived angular scattering maps for the reaction O($^1$D) + $H_2 \rightarrow$ OH($v', j'$) + H .[13] Part (a) is specific to the OH($j' = 0$–10) products in $v' = 0$, whilst part (b) is for the $j' = 0$–17 products in $v' = 4$. The data can be compared with the experimental OH state-specific scattering maps obtained for the O($^1$D) + $CH_4$ shown in Fig. 14.

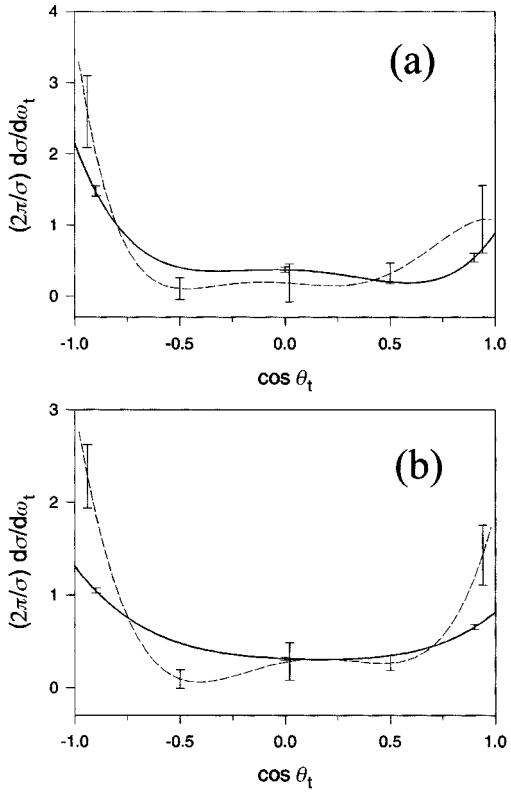


**Fig. 13** Comparison between the experimental (bold line) and QCT calculated (dashed line) angular distribution for the reaction O($^1$D) + $H_2 \rightarrow$ OH($v' = 0, N'$) + H.[26] Part (a) is for the $N' = 5$ products, whilst part (b) is for the $N' = 14$ products.

increased moment of inertia in ($CH_3OH$) compared to (HOH), suggests a considerable increase in the relevant time-scales.

The rotational period provides a 'clock' against which the lifetime of the intermediate collision complex can be measured. Channels with intermediate lifetimes longer than the mean rotational period will be expected to display symmetric product angular distributions. The problem is, how to measure the absolute 'clock rate' and thereby, 'time' the reactive events. One way, is to use an ultrafast laser to probe the rate of appearance of the scattered products directly, on a femtosecond time-scale. This has actually been done by Stephenson and van Zee,[35] who probed the rate of appearance of $OH|v' = 0, j'\rangle$ from a ($CH_3OH$) collision complex, prepared by photolysis of $O_3$ [the source of $O(^1D)$], bound to $CH_4$ in a van der Waals complex generated in the low temperature environment of a molecular beam expansion. The result indicates a transient complex lifetime $\langle\tau_d\rangle \simeq 3$ ps. Unfortunately, the corresponding time-scales for the analogous reaction with $H_2$ are too fast to allow a similar, direct measurement. There is a way out, however, *via* simulations using classical trajectory calculations. They indicate rotational periods $\langle\tau_r\rangle \simeq 100$ fs but (HOH) lifetimes increasing from $\langle\tau_d\rangle \simeq 30$ fs to 85 fs for decomposition into $OH|v' = 0\rangle$ to $|v' = 4\rangle$, fully consistent with the change in the angular distribution from backward scattering to near symmetric. For OH scattered into the higher vibrational levels $|v' = 4\rangle$, the lifetimes $\langle\tau_d\rangle \simeq \langle\tau_r\rangle$, and the angular distributions display nearly equal forward and backward peaks. When the OH fragments are scattered into the lowest quantum states $|v' = 0\rangle$, the complex lifetime $\langle\tau_d\rangle \leqslant \langle\tau_r\rangle$, and the fragments scatter predominantly into the backward hemisphere because the intermediates make, on average, less than a full rotation before they proceed to products. The real-time and rotational clocks used to analyse the results for the reaction of $O(^1D_2)$ with $CH_4$ indicated time-scales in the picosecond rather than the femtosecond range—time enough for extensive vibrational energy redistribution into the $CH_3$ fragment and associated no doubt, with the larger moment of inertia of the rotating ($CH_3OH$) complex. Nevertheless, the remarkable similarity between the two sets of scattering data (Fig. 12 and 14) suggests that the *relative* time-scales, $\langle\tau_d\rangle/\langle\tau_r\rangle$, in the channels generating OH $|v' = 0\rangle$ and $|v' = 4\rangle$, are little changed when $CH_4$ is substituted for $H_2$.

We turn now to the collisional energy dependence of the reaction. If there is truly no barrier in the entrance channel, the reaction probability, measured by the cross-section, $\sigma_R$, should actually decrease with increasing collision energy. $O(^1D)$ atoms approaching the target molecule at long range (large impact parameters) may still be drawn into the 'reaction field' provided they are not travelling too rapidly. If they are, then they may avoid reaction because their momentum can carry them out of harm's way. To be captured they would need to follow a closer trajectory (with a smaller impact parameter). The 'reactive' cross-sectional area presented by the target will shrink at elevated collision energies and the '*excitation function*', $\sigma_R(E_t)$, should fall as the collision energy, $E_t$, increases. This is precisely the behaviour observed.[31] Fig. 15 shows the excitation function for the scattering of $OH|v' = 0\rangle$ from collisions of $O(^1D)$ with $H_2$, determined through analysis of its Doppler-resolved spectral band contours; it compares very well with the simulation based upon classical trajectories over the *ab initio* potential energy surface for the *ground* electronic state of the collision complex.

Suppose the reactive collisions had proceeded instead, over the initially repulsive electronically excited potential energy surface(s). In this situation, increasing collision energy should increase the probability of reaction; once the energy was sufficient to overcome the initial barrier the excitation function would be expected to increase, monotonically, from a threshold value. Trajectory simulations for this pathway[32] also predict totally different patterns of energy and momentum disposal in the scattered products, with abstraction favouring high vibrational excitation and low rotation (the inverse of the distribution generated *via* an insertion pathway over the ground electronic

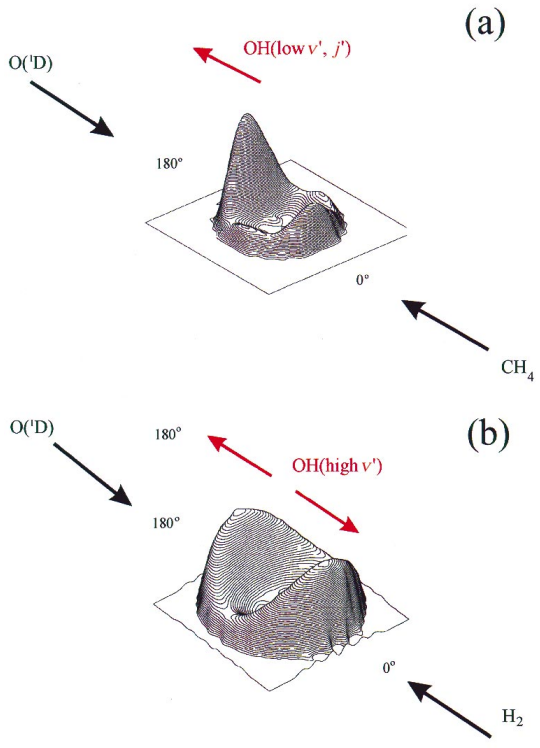


**Fig. 14** The experimentally derived angular scattering maps for the reaction $O(^1D) + CH_4 \rightarrow OH(v', j') + CH_3$. Part (a) is for $OH(v' = 0, N' = 5, A')$, and part (b) is for $OH(v' = 4, N' = 8)$. The data on which the plots are based is taken from reference 16.

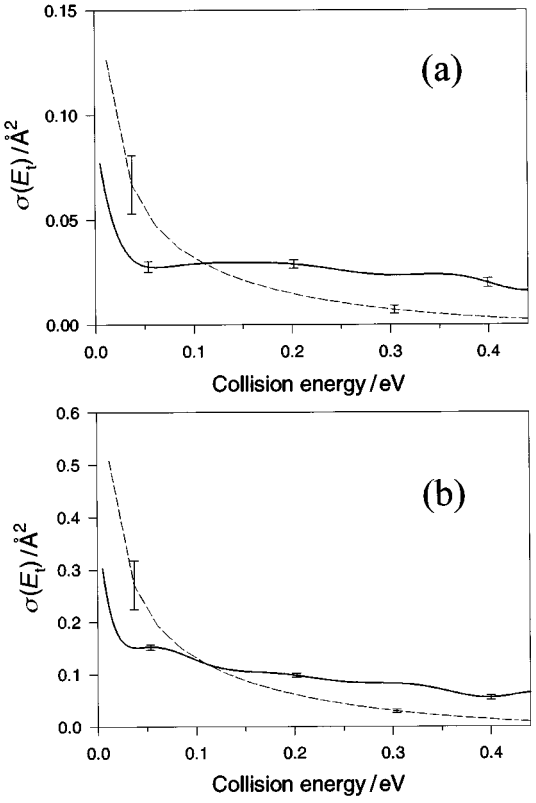


**Fig. 15** Comparison between the experimental (bold line) and QCT calculated (dashed line) state-resolved excitation functions, $\sigma_R(E_t)$, for the reaction $O(^1D) + H_2 \rightarrow OH(v' = 0, N') + H$, leading to OH products in $N' = 5$ (a) and $N' = 14$ (b).[26]

potential energy surface) and a strongly backward scattered angular distribution. Although some experimental evidence has been presented in favour of this alternative, abstraction pathway at elevated collision energies, its actual (or even real) contribution remains to be established.[31,32]

## 5 Forward look

The case histories presented above illustrate the power of the new stereodynamical methods in exploring the intimate details of individual reactive molecular collisions. In the past three or four years, experimental procedures have been optimised, and the new results obtained have revealed many new features of *state-resolved* reaction dynamics which were hitherto unforeseen. Diversity, rather than conformity, appears to be the rule; each reactive channel displays its own unique dynamical signature.

Particularly exciting discoveries are being made in areas where experiment and theory interact most closely, and the results from the new experiments are proving a demanding test of *ab initio* theory. It is perhaps sobering that many dynamical aspects of the 'simple' gas phase reaction $O(^1D) + H_2$ remain to be rationalised: theoretical studies of this reaction highlight the current 'state-of-the-art' in *ab initio* theory. Following in the footsteps of Herschbach and co-workers,[6,7] theorists and experimentalists are beginning to turn increasingly to angular momentum polarisation to provide additional insights into reaction mechanism. Such studies will help maintain (for some, at least) the 'buzz and passion' which animates the world of molecular reaction dynamics.

## 6 Acknowledgements

It is a pleasure to thank our past and present colleagues whose work has contributed to this Review Article, and to acknowledge particularly Professor Javier Aoiz, at the Complutense University, Madrid, with whom we have enjoyed a long and fruitful collaboration.

## 7 References

1 D. M. Neumark, A. M. Wodtke, G. N. Robinson, C. C. Hayden and Y. T. Lee, *J. Chem. Phys.*, 1985, **82**, 3045.
2 D. E. Manolopoulos, *J. Chem. Soc. Faraday Trans.*, 1997, **93**, 673, and references therein.
3 E. J. Murphy, J. H. Brophy, G. S. Arnold, W. L. Dimpfl and J. L. Kinsey, *J. Chem. Phys.*, 1979, **70**, 5910.
4 P. L. Houston, *Acc. Chem. Res.*, 1995, **28**, 453.
5 R. N. Zare and D. R. Herschbach, *Proc. IEEE*, 1963, **51**, 173; P. L. Houston, *J. Phys. Chem.*, 1987, **91**, 5388, and J. P. Simons, *ibid*, 5378.
6 D. E. Case and D. R. Herschbach, *Mol. Phys.*, 1975, **30**, 1537, and references therein.
7 D. E. Case, G. M. McClelland and D. R. Herschbach, *Mol. Phys.*, 1978, **35**, 541.
8 Published in *J. Phys. Chem.*, 1987, **91**, 5365 to 5515. See, in particular, the opening review by R. B. Bernstein, D. R. Herschbach and R. D. Levine, *ibid*, 5365.
9 C. H. Greene and R. N. Zare, *J. Chem. Phys.*, 1983, **78**, 6742.
10 R. N. Dixon, *J. Chem. Phys.*, 1986, **85**, 1866.
11 B. Katz, J. Park, S. Satyapal, S. Tasaki, A Chattopadhyay, W. Yi and R. Bersohn, *Faraday Discuss. Chem. Soc.*, **91**, 73.
12 A. J. Orr-Ewing and R. N. Zare, in *Chemical dynamics and kinetics of small free radicals*, eds. K. Liu and A. L. Wagner, World Scientific, Singapore, 1995, Part II, p. 936; A. J. Orr-Ewing and R. N. Zare, *Annu. Rev. Phys. Chem.*, 1994, **45**, 315; A. J. Orr-Ewing, *J. Chem. Soc. Faraday Trans.*, 1996, **92**, 881, and references therein.
13 M. Brouard and J. P. Simons, in *Chemical dynamics and kinetics of small free radicals*, eds. K. Liu and A. L. Wagner, World Scientific, Singapore, 1995, Part II, p. 936; J. P. Simons, *J. Chem. Soc. Faraday. Trans.*, 1997, **93**, 4095 and references therein.
14 F. J. Aoiz, M. Brouard, P. A. Enriquez and R. Sayos, *J. Chem. Soc. Faraday Trans.*, 1993, **89**, 1427.
15 N. E. Shafer, A. J. Orr-Ewing, W. R. Simpson, H. Xu, and R. N. Zare, *Chem. Phys. Lett.*, 1993, 212, 155; W. R. Simpson, A. J. Orr-Ewing and R. N. Zare, *ibid.*, 163.
16 M. Brouard, H. M. Lambert, C. L. Russell, J. Short and J. P. Simons, *Faraday Discuss. Chem. Soc.*, 1995, **102**, 179.
17 M. Brouard, H. M. Lambert, S. P. Rayner and J. P. Simons, *Mol. Phys.*, 1996, **89**, 403.
18 M. Brouard, I. Burak, G. A. J. Markillie, K. McGrath and C. Vallance, *Chem. Phys. Lett.*, **281**, 97.
19 N. E. Shafer, A. J. Orr-Ewing and R. N. Zare, *J. Phys. Chem.*, 1995, **99**, 7591.
20 F. J. Aoiz, M. Brouard and P. A. Enriquez, *J. Chem. Phys.*, 1996, **105**, 4981.
21 T. P. Rakitzis, S. A. Kandel and R. N. Zare, *J. Chem. Phys.*, 1997, **107**, 9382; T. P. Rakitzis, S. A. Kandel, T. Lev-On and R. N. Zare, *ibid.*, 9392.
22 F. J. Aoiz, M. Brouard, V. J. Herrero, V. Saez Rabanos and K. Stark, *Chem. Phys. Lett.*, 1997, **264**, 487.
23 M. P. de Miranda and D. C. Clary, *J. Chem. Phys.*, 1997, **106**, 4509, and references therein .
24 H. L. Kim, M. A. Wickramaaratchi, X. Zheng and G. E. Hall, *J. Chem. Phys.*, 1994, **101**, 2033; R. Fei, X. S. Zheng and G. E. Hall, *J. Phys. Chem.*, 1997, **101**, 2541.
25 A. J. Alexander, M. Brouard, S. P. Rayner and J. P. Simons, *Chem. Phys.*, 1996, **207**, 215.
26 A. J. Alexander, F. J. Aoiz, L. Bañares, M. Brouard, J. Short and J. P. Simons, *J. Phys. Chem.*, 1997, **101**, 7544.
27 A. J. Orr-Ewing, W. R. Simpson, T. P. Rakitzis, S. A. Kandel, and R. N. Zare, *J. Chem. Phys.*, 1997, **106**, 5961.
28 F. P. Gilbert, G. Maitland, A. Watson and K. G. McKendrick, *J. Chem. Soc. Faraday Trans.*, 1993, **89**, 1527.
29 F. Green, G. Hancock and A. J. Orr-Ewing, *Faraday Discuss. Chem. Soc.*, 1991, **91**, 79; D. Summerfield, M. L. Costen, G. A. D. Ritchie, G. Hancock, T. W. R. Hancock and A. J. Orr-Ewing, *J. Chem. Phys.*, 1997, **106**, 1391; M. L. Costen, D.Phil. Thesis, University of Oxford, 1997.
30 W. R. Simpson, T. P. Rakitzis, S. A. Kandel, A. J. Orr-Ewing and R. N. Zare, *J. Chem. Phys.*, 1995, **103**, 7299 and 7313; W. R. Simpson, T. P. Rakitzis, S. A. Kandel, T. Lev-On and R. N. Zare, *J. Phys. Chem.*, 1996, **100**, 7938.
31 A. J. Alexander, F. J. Aoiz, M. Brouard and J. P. Simons, *Chem. Phys. Lett.*, 1996, **256**, 561; A. J. Alexander, F. J. Aoiz, M. Brouard, I. Burak, Y. Fujimura, J. Short and J. P. Simons, *ibid.*, **262**, 589; A. J. Alexander, D. A. Blunt, M. Brouard, J. P. Simons, F. J. Aoiz, L. Banares, Y. Fujimura and M. Tsubouchi, *Faraday Discuss. Chem. Soc.*, 1998, **108**, 375.
32 T.-S. Ho, T. Hollebeek, H. Rabitz, L. B. Harding and G. C. Schatz, *J. Chem. Phys.*, 1996, **105**, 10472; G. C. Schatz, A. Papaioannou, L. A. Pederson, L. B. Harding, T.-S. Ho, T. Hollebeek and H. Rabitz, *ibid.*, 1997, **107**, 2340; G. C. Schatz, L. A. Pederson and P. J. Kuntz, *Faraday Discuss. Chem. Soc.*, 1998, **108**, 357.
33 H. Arai, S. Kato and S. Koda, *J. Phys. Chem.*, 1994, **98**, 12.
34 R. J. Buss, P. Casavecchia, T. Hirooka, S. J. Sibener and Y. T. Lee, *Chem. Phys. Lett.*, 1981, **82**, 386.
35 R. D. van Zee and J. C. Stephenson, *J. Chem. Phys.*, 1995, **102**, 6946.

*Received 4th June 1998*
*Accepted 13th July 1998*